Article

Journal of Vibration and Control
2017, Vol. 23(4) 673–692

DOI: 10.1177/1077546315581943
journals.sagepub.com/home/jvc
SAGE

Vibration and acoustic radiation of an orthotropic composite cylindrical shell in a hygroscopic environment

Xin Zhao, Bo Zhang and Yueming Li

Abstract

An analytical study is presented for vibration and acoustic radiation of a finite thin orthotropic composite cylindrical shell excited by a harmonic concentrated force in a hygroscopic environment. The modal analysis method is used to solve the governing equations. Theoretical results are presented in natural vibration, radial quadratic velocity, sound power and radiation efficiency, with uniform incremental moisture content. Furthermore, different stiffness, length and thickness are set respectively to research the effects of the material and structure parameters variation of the orthotropic cylindrical shell on the vibration and acoustic radiation characteristics. It is found that the natural frequencies decrease with an increase of moisture content. The modal indices associated with the lowest frequency mode reaches the modal indices corresponding to the lowest buckling mode near the critical buckling moisture content with moisture content. The radial quadratic velocity and sound radiation power decrease with the incremental moisture content in the lower frequency band. The vibration and acoustic response decrease with the enhanced stiffness. The increasing length has little impact on the sound radiation and the thickened cylindrical shell weakens the sound radiation response.

Keywords

Vibration, acoustic radiation, orthotropic, cylindrical shell, hygroscopic environment

1. Introduction

The thin orthotropic composite shells have many applications in the aerospace industry such as aircraft, missiles and launchers. The composite structures are typically exposed to moist environment in the aerospace industry, especially in the long-term storage period. The matrix in an orthotropic composite cylindrical shell is more susceptible to the hygroscopic condition than the fiber, and the hygroscopic strains and stresses are not equal in the longitudinal and circumferential axes due to the different moisture expansion coefficients. Hygroscopic stresses due to the moisture absorbed during the long-term storage period may induce buckling and dynamic instability in structures, and the pre-stress effect of hygroscopic load will affect the dynamic behavior of the structure, and then cause the changes of acoustic radiation characteristics.

Some researchers have studied buckling and free vibration behavior of composite cylindrical shells/shell panels due to hygroscopic load. Shen (2001) investigated the effect of hygroscopic conditions on the buckling and post-buckling of shear deformable laminated cylindrical shells subjected to combined loading of axial compression and external pressure. The results showed that the hygroscopic environment had a significant effect on the interactive buckling load as well as post-buckling response of the shell. Parhi et al. (2001) investigated the free vibration and transient response analysis of multiple delaminated doubly curved composite shells subjected to a hygroscopic environment by a quadratic isoparametric finite

State Key Laboratory for Strength and Vibration of Mechanical Structures, School of Aerospace Engineering, Xi'an Jiaotong University, China

Received: 27 November 2014; accepted: 16 March 2015

Corresponding author:
Yueming Li, State Key Laboratory for Strength and Vibration of Mechanical Structures, School of Aerospace Engineering, Xi'an Jiaotong University, No. 28 Xianning West Road, Xi'an, 710049, China.
Email: liyueming@mail.xjtu.edu.cn

element formulation based on the first order shear deformation theory. The results showed that the degradation in the natural frequencies and the increase in the amplitude of dynamic displacements and stresses are influenced by the degree of moisture concentration. Naidu and Sinha (2007) analyzed nonlinear free vibration behavior of laminated composite shells subjected to hygroscopic environments using the finite element method. They found that the fundamental frequencies reduce with the increase of moisture concentration levels. The effect in a thin shell panel is significant when it is subjected to uniform moisture concentration, and the panel becomes unstable at higher moisture concentration.

A lot of models have been developed by many researchers to study the acoustic radiation of the plate and cylindrical shell. Stepanishen (1982) presented an approach to evaluate the pressure field and vibratory response of a finite fluid-loaded cylindrical shell with infinite rigid extension which were connected to the shell. As a result of the importance of the acoustic self radiation and interaction impedances, the characteristics of impedances were investigated. They found that the acoustic self-impedances provide a resistive and inertial loading on the shell which will in general lower the natural frequency and the quality factor of each mode. Burroughs (1984) derived analytical expressions for the far field acoustic radiation from a point-driven circular cylindrical shell reinforced by doubly periodic rings. The results show two mechanisms of radiation: radiation from low wave numbers in the structural near field of the source; and scattering by the rings of structural energy from high-to-low wave numbers. Laulagnet and Guyader (1989) presented a modal analysis study of acoustic radiation by a finite cylindrical shell immersed in air or water. Theoretical results for shell power radiation, radial quadratic velocity and radiation efficiency had been given and analyzed by using the concept of evenly damped modes. Lyrintzis and Bofilios (1990) presented an analytical study to predict dynamic response and noise transmission of discretely stiffened multi-layered composite panels, and examined the effects of the temperature and high humidity. The results indicate that thermal and moisture effects are very important in predicting deflections and transmitted noise. Xie and Luo (1995) studied acoustic radiation properties of ring-stiffened cylindrical shell in fluids by means of Hamilton's principle and the Green function. The effects of hydrostatic pressure and rings on the acoustic radiation of the shells were discussed. Wang and Lai (2000) investigated a detailed acoustical analysis of the sound power produced by finite length acoustically thick circular cylindrical shells under mechanical excitation. Analysis of acoustically thick shells showed that unlike flat plates, for frequencies below the critical frequency, both supersonic and subsonic modes can exist. Consequently, the radiation efficiency is dependent on the geometries and boundary conditions and could reach unity at a frequency much lower than the critical frequency. Wang and Lai (2001) investigated the end effects of the length and the boundary conditions on the acoustic behavior of a circular cylindrical shell. They inferred that the boundary conditions affect the modal radiation efficiencies very much in the subsonic region. However, it has been shown that there exists a condition under which the end effects could be neglected for modal radiation efficiencies so that the infinite model could be used with fair accuracy. Daneshjou et al. (2009) explored the sound transmission through an infinite orthotropic composite cylindrical shell in the context of air-borne sound into the aircraft interior. They found that the decreasing of incident angle tends to enhance the transmission losses of cylinder in the stiffness-controlled region (below the ring frequency) and the coincidence frequency is shifted downwards. In higher altitude, acoustic impedance mismatch increases. Therefore, transmission losses in all broadband frequencies are enhanced. The discrete singular convolution (DSC) method is adopted by Civalek (2013) and Civalek and Gürses (2009) to analyze the free vibration of rotating cylindrical shells and laminated composite conical shells, which proves a controllable numerical accuracy by using the suitable bandwidth. Being a non-iterative method, the DSC method is relatively less computationally intensive. Also the DSC method gives reasonably accurate values for frequencies and mode shapes. Liao et al. (2011) developed an approximate analytic method to study sound radiation characteristics of a finite submerged axial periodically stiffened cylindrical shell excited by radial harmonic forces. They found that the axial stiffener number has just a slight influence on radiated sound power, whereas structural damping has a great influence on radiated power and radial quadratic velocity on the surface of the shell. Jeyaraj et al. (2008, 2011) adopted commercial finite element software to study the vibration and acoustic response characteristics of the isotropic plate and cylindrical shell under a thermal environment, respectively. They found that there is a significant change in the vibration mode shapes and ring frequency towards the lowest natural frequency with an increase with temperature in the study of the cylindrical shell, and then there is a sudden increase in overall sound power level near the critical buckling temperature, and significant changes in mode shapes with temperature do not affect the overall sound power level. Cao et al. (2012) studied the sound radiation from shear deformable stiffened laminated cylindrical shells in terms of sound pressure and the helical wave spectra. The far field sound pressure was derived by using the Fourier wave number transform and stationary phase method. It is shown that the dynamic stiffness of a ring taking into account the shear deformation is much lower than that of a ring modeled by the classical beam theory in the large circumferential wave numbers. Zhao et al. (2013) made a theoretical investigation of the vibration and acoustic response characteristics of an orthotropic laminated composite plate in a hygroscopic environment. The initial hygroscopic stress and mass addition caused by material moisture absorption are considered in the governing equations of the orthotropic plate. They found the dynamic response and sound radiation float to lower frequencies with elevated moisture content and the coincidence frequency decreases with the enhanced stiffness. The sound radiation efficiency of a vibrating, thin, elastically supported annular plate embedded into a flat rigid baffle was investigated by Rdzanek et al. (2014). The free axisymmetric time harmonic vibrations had been considered for a single mode. The presented formulations of sound radiation efficiency of an elastically supported annular plate are useful for numerical calculations within the low frequency range.

Solving the problem analytically is limited to certain conditions; it may be solved using numerical approaches such as the popular element-free methods that can provide a solution which cannot be obtained by the analytical method. Zhang and Liew (2014b) propose an improved moving least-squares–Ritz (IMLS–Ritz) method with its element-free framework developed for studying two-dimensional elasticity problems. Using the IMLS approximation for the field variables, the discretized governing equations of the problem are derived via the Ritz procedure. Zhang and Liew (2014a) also proposed an improved complex variable moving least-squares–Ritz (ICVMLS–Ritz) method for predicting a numerical solution of the two-dimensional nonlinear Schrödinger equation. In this element-free solution procedure, the ICVMLS approximation is employed to reduce the number of unknown coefficients in the trial function. Zhang et al. (2014) present a numerical study of the two-dimensional Schrödinger equation that is carried out using the improved complex variable element-free Galerkin (ICVEFG) method. The ICVEFG method involves employment of the improved complex variable moving least-squares (ICVMLS) in the element-free Galerkin (EFG) procedure for numerical approximation.

Although there is abundant literature for the analytical study of vibro-acoustic behavior of isotropic or stiffened cylindrical shells, very few studies have looked at vibration and sound radiation characteristics for the orthotropic cylindrical shell under hygroscopic environment. The uniform elevated moisture content may not occur in practice for the moisture content may vary according to the nature of surrounding, but the approximate uniform moisture content may occur after a long-term storage period. In the current study, vibration and acoustic response of a thin orthotropic circular composite cylindrical shell under uniform hygroscopic environment subjected to steady state excitations is investigated. A theoretical solution considering the effects of hygroscopic stress and mass addition caused by moisture absorption is obtained based on the improved Donnell type shell equation, with simply supported boundary conditions at the two ends of the shell which were terminated by infinite rigid cylindrical baffles. To examine the validity of the present solution, comparisons are made against the radial quadratic velocity and radiated power with the previous work for a finite long isotropic cylindrical shell. The natural frequency characteristic, radial quadratic velocity, radiated power and radiation efficiency of the orthotropic cylindrical shell with incremental moisture content are analysed. The influences of the stiffness, length and thickness of the orthotropic cylindrical shell on the vibration and acoustic responses are also discussed.

2. Formulation

Consider a finite thin orthotropic cylindrical shell in a hygroscopic environment, as shown in Figure 1, terminated by infinite rigid cylindrical baffles. The radius, thickness and length of the cylindrical shell is R, h and L respectively. The mass density of air is ρ_0, and the speed of sound in air is c_0. The shell is excited by harmonic point force $F(x, \theta, t)$. The variables x, θ, z refer to the axial, circumferential and radial directions. The variables u, v, w refer to displacement components in x, θ, z directions respectively. The cylindrical shell is composed of N layer laminas, and all laminas are orthotropic and the material principal directions are coincident with the coordinate system, so the composite cylindrical shell bonding together with the lamina having the same principal coordinate system can be assumed to be an orthotropic composite cylindrical shell. In the present study, based on the Kirchhoff–Love hypothesis, classical thin shell theory will be adopted in the analysis.

2.1. In-plane force induced by hygroscopic stress

Taking no account of the change of the moisture content, the internal force and moment of the shell element can be written as (Brush and Almroth, 1975):

$$\{N, M\} = \left\{[N_x, N_\theta, N_{x\theta}]^T, \quad [M_x, M_\theta, M_{x\theta}]^T\right\}$$

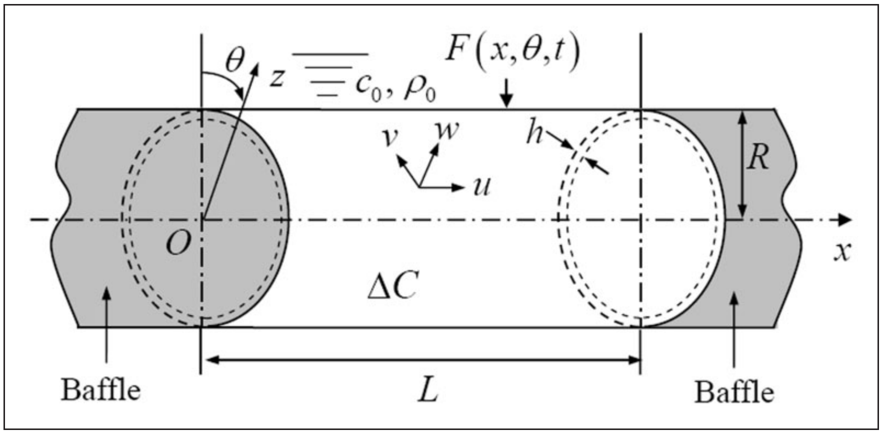

Figure 1. Cylindrical shell and co-ordinate system.

$$= \int_{-h/2}^{h/2} \left\{ [\sigma_x, \sigma_\theta, \sigma_{x\theta}]^T, \quad [\sigma_x z, \sigma_\theta z, \sigma_{x\theta} z]^T \right\} \mathrm{d}z \tag{1}$$

where N_x, N_θ, $N_{x\theta}$, M_x, M_θ and $M_{x\theta}$ are the forces and moments per unit length of shell element in normal and shear directions; σ_x, σ_θ and $\sigma_{x\theta}$ are the normal and shear stresses respectively. The state of plane stress of the orthotropic shell can be expressed as:

$$\begin{Bmatrix} \sigma_x \\ \sigma_\theta \\ \sigma_{x\theta} \end{Bmatrix} = \begin{bmatrix} Q_{11} & Q_{12} & 0 \\ Q_{12} & Q_{22} & 0 \\ 0 & 0 & Q_{66} \end{bmatrix} \begin{Bmatrix} \varepsilon_x \\ \varepsilon_\theta \\ \gamma_{x\theta} \end{Bmatrix} \tag{2}$$

where Q_{11}, Q_{22}, Q_{12} and Q_{66} are the transformed reduced stiffness which are related to the usual engineering parameters in the following way:

$$Q_{11} = \frac{E_1}{(1 - \mu_{12}\mu_{21})} \tag{3a}$$

$$Q_{22} = \frac{E_2}{(1 - \mu_{12}\mu_{21})} \tag{3b}$$

$$Q_{12} = \frac{\mu_{12} E_2}{(1 - \mu_{12}\mu_{21})} \tag{3c}$$

$$Q_{66} = G_{12} \tag{3d}$$

where E_1 and E_2 are the longitudinal and tangential Young's modulus, respectively, G_{12} is the shear modulus, μ_{12} and μ_{21} are Poisson's ratios.

The normal and shear strains at a point with distance z from the middle surface of the shell according to the Kirchhoff–Love assumptions are (Brush and Almroth, 1975):

$$\varepsilon_x = \varepsilon_{xm} + z k_x \tag{4a}$$

$$\varepsilon_\theta = \varepsilon_{\theta m} + z k_\theta \tag{4b}$$

$$\gamma_{x\theta} = \gamma_{x\theta m} + z k_{x\theta} \tag{4c}$$

where the subscript m refers to the strains on the middle surface of the shell; k_x and k_θ are the bending strains in the axial direction x and circumferential direction θ, respectively; and $k_{x\theta}$ is the twist strain in the $x\theta$ plane. The general linear strain–displacement relations can be given in the following terms for the strains on the middle surface and the curvatures in terms of the displacement component u, v and w in the axial, circumferential, and normal to the middle plane directions:

$$\varepsilon_{xm} = \frac{\partial u}{\partial x} \tag{5a}$$

$$\varepsilon_{\theta m} = \frac{1}{R}\frac{\partial v}{\partial \theta} + \frac{w}{R} \tag{5b}$$

$$\gamma_{x\theta m} = \frac{1}{R}\frac{\partial u}{\partial \theta} + \frac{\partial v}{\partial x} \tag{5c}$$

$$k_x = -\frac{\partial^2 w}{\partial x^2} \tag{5d}$$

$$k_\theta = \frac{1}{R^2}\left(\frac{\partial v}{\partial \theta} - \frac{\partial^2 w}{\partial \theta^2}\right) \tag{5e}$$

$$k_{x\theta} = \frac{1}{2R}\left(\frac{\partial v}{\partial x} - 2\frac{\partial^2 w}{\partial x \partial \theta}\right) \tag{5f}$$

Considering that based on the thin shell theory, the internal force and moment of the shell element with the linear strain–displacement relations can be obtained:

$$N = \begin{Bmatrix} N_x \\ N_\theta \\ N_{x\theta} \end{Bmatrix} = \int_{-h/2}^{h/2} \begin{Bmatrix} \sigma_x \\ \sigma_\theta \\ \sigma_{x\theta} \end{Bmatrix} \mathrm{d}z$$

$$= \begin{bmatrix} K_{11} & K_{12} & 0 \\ K_{12} & K_{22} & 0 \\ 0 & 0 & K_{66} \end{bmatrix} \begin{Bmatrix} \varepsilon_{xm} \\ \varepsilon_{\theta m} \\ \gamma_{x\theta m} \end{Bmatrix} \tag{6a}$$

$$M = \begin{Bmatrix} M_x \\ M_\theta \\ M_{x\theta} \end{Bmatrix} = \int_{-h/2}^{h/2} \begin{Bmatrix} \sigma_x \\ \sigma_\theta \\ \sigma_{x\theta} \end{Bmatrix} z\mathrm{d}z$$
$$= \begin{bmatrix} D_{11} & D_{12} & 0 \\ D_{12} & D_{22} & 0 \\ 0 & 0 & D_{66} \end{bmatrix} \begin{Bmatrix} k_x \\ k_\theta \\ k_{x\theta} \end{Bmatrix} \tag{6b}$$

where $K_{ij}(i,j = 1,2,6)$ and $D_{ij}(i,j = 1,2,6)$ are membrane stiffness and bending stiffness are written as below:

$$K_{11} = \frac{E_1 h}{(1 - \mu_{12}\mu_{21})} \tag{7a}$$

$$K_{22} = \frac{E_2 h}{(1 - \mu_{12}\mu_{21})} \tag{7b}$$

$$K_{12} = \frac{\mu_{12} E_2 h}{(1 - \mu_{12}\mu_{21})} \tag{7c}$$

$$K_{66} = G_{12} h \tag{7d}$$

$$D_{11} = \frac{E_1 h^3}{12(1 - \mu_{12}\mu_{21})} \tag{7e}$$

$$D_{22} = \frac{E_2 h^3}{12(1 - \mu_{12}\mu_{21})} \tag{7f}$$

$$D_{12} = \frac{\mu_{12} E_2 h^3}{12(1 - \mu_{12}\mu_{21})} \tag{7g}$$

$$D_{66} = \frac{G_{12} h^3}{12} \tag{7h}$$

There will be in-plane force induced by hygroscopic stress in orthotropic shell when the hygroscopic environment changes from initial uniform moisture content to a final value. In this condition, there is no in-plane and radial displacement. The hygroscopic stress–strain relation (Kaw, 2006; Whitney and Ashton, 1971) can be written as:

$$\begin{Bmatrix} \sigma_x^C \\ \sigma_\theta^C \\ \sigma_{x\theta}^C \end{Bmatrix} = \begin{bmatrix} Q_{11} & Q_{12} & 0 \\ Q_{12} & Q_{22} & 0 \\ 0 & 0 & Q_{66} \end{bmatrix} \begin{Bmatrix} \varepsilon_x^C \\ \varepsilon_\theta^C \\ 0 \end{Bmatrix} \tag{8}$$

where the subscript C refers to the hygroscopic stress induced by the moisture content difference. Note that no shearing strains are induced in the material axes. The moisture change induced strains ε_x^C, ε_θ^C are given by:

$$\begin{Bmatrix} \varepsilon_x^C \\ \varepsilon_\theta^C \\ 0 \end{Bmatrix} = \Delta C \begin{Bmatrix} \beta_1 \\ \beta_2 \\ 0 \end{Bmatrix} \tag{9}$$

where β_1 and β_2 are the axial and circumferential coefficients of hygroscopic expansion in the principal material directions, respectively. $\Delta C(\%) = C_f - C_i$ is denoted as the moisture content change, and $C_i(\%)$ and $C_f(\%)$ is the initial and final uniform moisture content in the orthotropic shell. The hygroscopic force and moment could be written as below:

$$N^C = \begin{Bmatrix} N_x^C \\ N_\theta^C \\ N_{x\theta}^C \end{Bmatrix} = \int_{-h/2}^{h/2} \begin{Bmatrix} \sigma_x^C \\ \sigma_\theta^C \\ \sigma_{x\theta}^C \end{Bmatrix} \mathrm{d}z$$
$$= \int_{-h/2}^{h/2} \begin{bmatrix} Q_{11} & Q_{12} & 0 \\ Q_{12} & Q_{22} & 0 \\ 0 & 0 & Q_{66} \end{bmatrix} \begin{Bmatrix} \varepsilon_x^C \\ \varepsilon_\theta^C \\ 0 \end{Bmatrix} \mathrm{d}z \tag{10a}$$

$$M^C = \begin{Bmatrix} M_x^C \\ M_\theta^C \\ M_{x\theta}^C \end{Bmatrix} = \int_{-h/2}^{h/2} \begin{Bmatrix} \sigma_x^C \\ \sigma_\theta^C \\ \sigma_{x\theta}^C \end{Bmatrix} z\mathrm{d}z$$
$$= \int_{-h/2}^{h/2} \begin{bmatrix} Q_{11} & Q_{12} & 0 \\ Q_{12} & Q_{22} & 0 \\ 0 & 0 & Q_{66} \end{bmatrix} \begin{Bmatrix} \varepsilon_x^C \\ \varepsilon_\theta^C \\ 0 \end{Bmatrix} z\mathrm{d}z \tag{10b}$$

The ends of the cylindrical shell terminated by infinite rigid cylindrical baffles are simply supported, and the boundary condition is given as:

$$v = w = \frac{\partial u}{\partial x} = \frac{\partial^2 w}{\partial x^2} = 0 \quad (x = 0, L) \tag{11}$$

If the shell is simply supported and the axial displacement is prevented, the moisture content can be uniformly raised to a final value C_f such that the shell buckles. To find the critical $\Delta C = C_f - C_i$, the prebuckling hygroscopic stresses are (Eslami and Javaheri, 1999; Eslami et al., 1996):

$$N_{x0} = N_x^C = -(K_{11}\beta_1 + K_{12}\beta_2)\Delta C \tag{12a}$$

$$N_{\theta 0} = N_{x\theta 0} = 0 \tag{12b}$$

N_{x0}, $N_{\theta 0}$ and $N_{x\theta 0}$ refer to the pre-stresses in longitudinal, tangential and shearing directions.

Thus the resultant force and moment of the shell element can be obtained as:

$$\left\{\bar{N}, \bar{M}\right\}^T = \left\{[N, M]^T - \left[N^C, M^C\right]^T\right\} \tag{13}$$

2.2. Vibration and acoustic response of the orthotropic cylindrical shell in a hygroscopic environment

According to the improved Donnell's shell theory (Brush and Almroth, 1975; Leissa, 1973), considering the additional mass by absorbing moisture (Lyrintzis and Bofilios, 1990; Zhao et al., 2013), a new motion equilibrium equation of the thin orthotropic cylindrical shell including the pre-stresses effect can be established as follows:

$$\frac{\partial N_x}{\partial x} + \frac{\partial N_{x\theta}}{R\partial\theta} = (1+\Delta C)\rho h \frac{\partial^2 u}{\partial x^2} \tag{14a}$$

$$\begin{aligned}&\frac{\partial N_{x\theta}}{\partial x} + \frac{\partial N_\theta}{R\partial\theta} + \frac{1}{R^2}\frac{\partial M_\theta}{\partial\theta} \\ &+ \frac{1}{R}\frac{\partial M_{x\theta}}{\partial x} + N_{\theta 0}\left(\frac{1}{R^2}\frac{\partial w}{\partial\theta} - \frac{v}{R^2}\right) \\ &+ N_{x\theta 0}\frac{1}{R}\frac{\partial w}{\partial x} = (1+\Delta C)\rho h \frac{\partial^2 v}{\partial x^2}\end{aligned} \tag{14b}$$

$$\begin{aligned}&\frac{\partial^2 M_x}{\partial x^2} + \frac{2}{R}\frac{\partial^2 M_{x\theta}}{\partial x\partial\theta} + \frac{1}{R^2}\frac{\partial^2 M_\theta}{\partial\theta^2} - \frac{1}{R}N_\theta \\ &+ N_{x0}\frac{\partial^2 w}{\partial x^2} + N_{x\theta 0}\left(\frac{2}{R}\frac{\partial^2 w}{\partial x\partial\theta} - \frac{1}{R}\frac{\partial v}{\partial x}\right) \\ &+ N_{\theta 0}\left(\frac{1}{R^2}\frac{\partial^2 w}{\partial\theta^2} - \frac{1}{R^2}\frac{\partial v}{\partial\theta}\right) = (1+\Delta C) \\ &\times \rho h \frac{\partial^2 w}{\partial x^2} - F(x,\theta,t) + p(x,\theta,t)\end{aligned} \tag{14c}$$

where ρ is the density of the material, ρh is the shell mass per unit area, and $(1+\Delta C)$ accounts for the absorbed moisture. $F(x,\theta,t)$ is the driving force; $p(x, \theta, t)$ is the shell boundary pressure.

For a simply supported cylindrical shell, the middle surface displacement can be expanded in a series of the shell modes (Junger and Feit, 1986) (for simplicity, time- dependent factor $e^{-j\omega t}$ will be suppressed throughout for a harmonic vibration):

$$u = \sum_{\lambda=0}^{1}\sum_{n=0}^{\infty}\sum_{m=1}^{\infty} U_{mn}^{\lambda}\sin\left(n\theta + \frac{\lambda\pi}{2}\right)\cos(k_m x) \tag{15a}$$

$$v = \sum_{\lambda=0}^{1}\sum_{n=0}^{\infty}\sum_{m=1}^{\infty} V_{mn}^{\lambda}\cos\left(n\theta + \frac{\lambda\pi}{2}\right)\sin(k_m x) \tag{15b}$$

$$w = \sum_{\lambda=0}^{1}\sum_{n=0}^{\infty}\sum_{m=1}^{\infty} W_{mn}^{\lambda}\sin\left(n\theta + \frac{\lambda\pi}{2}\right)\sin(k_m x) \tag{15c}$$

here $\lambda = 0$ (resp. 1) denotes antisymmetric (resp. symmetric) modes, U_{mn}^{λ}, V_{mn}^{λ} and W_{mn}^{λ} refer to the displacement amplitudes in axial, circumferential and radial directions, $k_m = m\pi/L$, n is circumferential order, m is the longitudinal order. Both the force and shell boundary pressure can be expanded in the displacement form respectively as:

$$F(x,\theta) = \sum_{\lambda=0}^{1}\sum_{n=0}^{\infty}\sum_{m=1}^{\infty} F_{mn}^{\lambda}\sin\left(n\theta + \frac{\lambda\pi}{2}\right)\sin(k_m x) \tag{16}$$

$$p(x,\theta) = \sum_{\lambda=0}^{1}\sum_{n=0}^{\infty}\sum_{m=1}^{\infty} P_{mn}^{\lambda}\sin\left(n\theta + \frac{\lambda\pi}{2}\right)\sin(k_m x) \tag{17}$$

and the modal expansion coefficient F_{mn}^{λ} and P_{mn}^{λ} can be written as:

$$F_{mn}^{\lambda} = \frac{\varepsilon_n}{\pi L}\int_0^{2\pi}\int_0^L F(x,\theta)\sin\left(n\theta + \frac{\lambda\pi}{2}\right)\sin(k_m x)\mathrm{d}x\mathrm{d}\theta \tag{18}$$

$$P_{mn}^{\lambda} = \frac{\varepsilon_n}{\pi L}\int_0^{2\pi}\int_0^L p(x,\theta)\sin\left(n\theta + \frac{\lambda\pi}{2}\right)\sin(k_m x)\mathrm{d}x\mathrm{d}\theta \tag{19}$$

where ε_n is the Neumann factor. To a radial point driving,

$$F_{mn}^{\lambda} = \frac{\varepsilon_n F_0}{\pi L R}\sin\left(n\theta_0 + \frac{\lambda\pi}{2}\right)\sin(k_m x_0) \tag{20}$$

where F_0 is the amplitude of the driving force, x_0 and θ_0 are the axial and circumferential coordinate for the driving force. Substituting equations (5a) to (5f) into equations (6a) and (6b), respectively, then substituting the result expressions and equations (12) and (15) to (17) into the motion equations (14), the modal equation can be obtained as below:

$$\begin{bmatrix} a_{11} & a_{12} & a_{13} \\ a_{21} & a_{22} & a_{23} \\ a_{31} & a_{32} & a_{33} \end{bmatrix}\begin{bmatrix} U_{mn}^{\lambda} \\ V_{mn}^{\lambda} \\ W_{mn}^{\lambda} \end{bmatrix} = \frac{R^2}{\rho c_m^2 h}\begin{pmatrix} 0 \\ 0 \\ F_{mn}^{\lambda} - P_{mn}^{\lambda} \end{pmatrix} \tag{21}$$

in which

$$a_{11} = \bar{m}^2 + \frac{G_{12}(1-\mu_{12}\mu_{21})}{E_1}n^2 - \Omega^2 \tag{22a}$$

$$a_{12} = a_{21} = \frac{\mu_{12}E_2 + G_{12}(1-\mu_{12}\mu_{21})}{E_1}\bar{m}n \tag{22b}$$

$$a_{13} = a_{31} = -\frac{\mu_{12}E_2}{E_1}\bar{m} \tag{22c}$$

$$a_{22} = \left(1+\frac{h^2}{24R^2}\right)\frac{G_{12}(1-\mu_{12}\mu_{21})}{E_1}\bar{m} + \left(1+\frac{h^2}{24R^2}\right)\frac{E_2}{E_1}n^2 - \Omega^2 \tag{22d}$$

$$a_{23} = a_{32} = -\frac{h^2}{12R^2}\left[\frac{\mu_{12}E_2 + G_{12}(1-\mu_{12}\mu_{21})}{E_1}\bar{m}^2 n + \frac{E_2}{E_1}n^3\right] + \frac{E_2}{E_1}n \tag{22e}$$

and

$$a_{33} = \frac{h^2}{12R^2}\left[\bar{m}^4 + 2\frac{\mu_{12}E_2 + G_{12} \times (1-\mu_{12}\mu_{21})}{E_1}\bar{m}^2n^2 + \frac{E_2}{E_1}n^4\right] + \frac{E_2}{E_1} - \left(\beta_1 + \frac{\mu_{12}E_2}{E_1}\beta_2\right)\bar{m}^2\Delta C - \Omega^2 \tag{22f}$$

where $\bar{m} = m\pi R/L$, $\Omega^2 = \omega^2R^2/c_m^2$, $c_m = [E_1/(1-\mu_{12}\mu_{21})(1+\Delta C)\rho]^{1/2}$. The coefficients a_{ij} $(i,j = 1,2,3)$ contain the coefficients of hygroscopic expansion and moisture content variation since the hygroscopic effect is introduced in the present paper, and the effect could be solved from equation (21) corresponding to each pair $(\bar{m}, n)$.

Setting P_{mn}^{λ} equal to zero in equation (21), the modal vibration velocity in vacuum can be derived as (Stepanishen, 1982):

$$\dot{W}_{mn}^{\lambda} = \frac{F_{mn}^{\lambda}}{Z_{mn}^{M}} = \frac{F_{mn}^{\lambda}(-j\omega)}{(1+\Delta C)\rho h\left[\omega_{mn}^2(1-i\eta) - \omega^2\right]} \tag{23}$$

where Z_{mn}^{M} is the mechanical impedance of the thin orthotropic shell and is equal to:

$$Z_{mn}^{M} = \frac{\left|a_{ij}\right|}{(-j\omega)\frac{R^2}{(1+\Delta C)\rho h c_m^2}\left[a_{11}a_{22} - a_{12}^2\right]} \tag{24}$$

ω_{mn} is the natural frequency in vacuum, and $j = \sqrt{-1}$, $\left|a_{ij}\right|$ is determinant of coefficient.

According to the transformation relation between the sound pressure and vibration velocity in wave number domain K, P_{mn}^{λ} denotes modal sound pressure coefficient widely known as:

$$P_{mn}^{\lambda} = \sum_q \dot{W}_{qn}^{\lambda} Z_{qmn}^{A} \tag{25}$$

where Z_{qmn}^{A} is the radiation impedance in wave number domain can be written as (Stepanishen, 1982; Laulagnet, 1989):

$$Z_{qmn}^{A} = \frac{jqm\rho_0\omega R^2\pi^2}{\varepsilon_n L^2}\int_{-\infty}^{+\infty}\frac{\left(1-(-1)^q e^{-jKL}\right)}{k_q^2 - K^2} \times \frac{\left(1-(-1)^m e^{jKL}\right)}{k_m^2 - K^2}\frac{1}{\sqrt{k_0^2 - K^2}R} \times \frac{H_n^{(1)}\left(\sqrt{k_0^2-K^2}R\right)}{H_n^{(1)\prime}\left(\sqrt{k_0^2-K^2}R\right)}\mathrm{d}K \tag{26}$$

where $k_0 = \omega/c_0$ is the acoustic wave number, $q = m$ is the self-impedance and $q \neq m$ is the interaction impedance. $H_n^{(1)}(z)$ is the nth-order Hankel function of the first kind. Laulagnet and Guyader (1989) pointed out that in the case of air the cross-modal coupling introduced by the fluid is very weak and does not significantly affect the results with regard to the radiated power and the shell quadratic velocity, while it shows that the cross-modal coupling can be neglected as a first approximation. Ignoring the interaction impedance effects on the vibration velocity, the radial vibration velocity in air can be written as (Stepanishen, 1982):

$$\dot{W}_{mn}^{\lambda} = \frac{F_{mn}^{\lambda}}{Z_{mn}^{M} + Z_{mmn}^{A}} \tag{27}$$

The sound radiation power can be derived as:

$$\prod(\omega) = \frac{1}{2}\int_s \mathrm{Re}[p(R,\theta,x)\dot{w}^*(\theta,x)]\mathrm{d}s = \frac{1}{2}\mathrm{Re}\left[\sum_{\lambda=0}^{1}\sum_{n=0}^{\infty}\sum_{m=1}^{\infty}\sum_{q=1}^{\infty}\dot{W}_{mn}^{\lambda}Z_{qmn}^{A}\left(\dot{W}_{qn}^{\lambda}\right)^*\right] \tag{28}$$

where the asterisk denotes complex conjugate. The radial quadratic velocity is

$$\left\langle\dot{w}(\theta,x)\dot{w}^*(\theta,x)\right\rangle = \frac{1}{4\varepsilon_n}\sum_{n=0}^{\infty}\sum_{m=1}^{\infty}\dot{W}_{mn}^{\lambda}\left(\dot{W}_{mn}^{\lambda}\right)^* \tag{29}$$

and then the sound radiation efficiency is obtained as:

$$\sigma(\omega) = \frac{\prod(\omega)}{\rho_0 c_0 S\left\langle\dot{w}(\theta,x)\dot{w}^*(\theta,x)\right\rangle} \tag{30}$$

where $S = 2\pi RL$ refer to the surface area of the cylindrical shell. In the following, radiated power and radial quadratic velocity are in dB respectively, referenced to 10^{-12} watt and 5×10^{-8} m/s in air.

2.3. Natural vibration of the orthotropic cylindrical shell in hygroscopic environment

In natural vibration, the shell is assumed to oscillate with a natural circular frequency ω. Setting the determinant of the coefficient of the modal equation (21) equal to zero, and expanding the determinant in terms of Ω^2 leads to a cubic equation for Ω^2:

$$\Omega^6 + C_1\Omega^4 + C_2\Omega^2 + C_3 = 0 \tag{31}$$

with

$$C_1 = -(a_{11} + a_{22} + a_{33})$$

$$C_2 = a_{11}a_{22} + a_{22}a_{33} + a_{11}a_{33} - \left(a_{12}^2 + a_{23}^2 + a_{13}^2\right)$$

and

$$C_3 = a_{11}a_{23}^2 + a_{22}a_{13}^2 + a_{33}a_{12}^2 - a_{11}a_{22}a_{33} - 2a_{12}a_{13}a_{23} \tag{32}$$

The solution of equation (31) is similar to (Soedel, 2004):

$$\Omega_{imn}^2 = -\frac{2}{3}\sqrt{C_1^2 - 3C_2 \cos\left[\delta + \frac{2\pi}{3}(i-1)\right]} - \frac{C_1}{3} \quad (i = 1, 2, 3) \tag{33}$$

in which

$$\delta = \frac{1}{3}\cos^{-1}\left[\frac{C_1^3 - 4.5C_1C_2 + 13.5C_3}{\left(C_1^2 - 3C_2\right)^{\frac{3}{2}}}\right] \tag{34}$$

For every m, n combination, there are thus three frequencies. The lowest is associated with the mode where the radial component dominates, while the other two are usually higher by an order of magnitude and are associated with the mode where the displacements in the tangent plane dominate.

2.4. Calculation for critical buckling moisture content

Under simply supported conditions and where the axial displacement is prevented, moisture content can be uniformly raised from initial moisture content $C_i(\%)$ to final value $C_f(\%)$ such that shell buckles. The entire hygroscopic load cases in the present study are designed below the critical buckling moisture content. The improved Donnell stability equations in terms of displacement components can be written as (Eslami and Javaheri, 1999):

$$RK_{11}\frac{\partial^2 u}{\partial x^2} + K_{12}\left(\frac{\partial^2 v}{\partial x \partial\theta} + \frac{\partial w}{\partial x}\right) + K_{66}\left(\frac{1}{R}\frac{\partial^2 u}{\partial\theta^2} + \frac{\partial^2 v}{\partial x\partial\theta}\right) = 0 \tag{35a}$$

$$\begin{aligned} &K_{12}\frac{\partial^2 u}{\partial x\partial\theta} + \frac{K_{22}}{R}\left(\frac{\partial^2 v}{\partial\theta^2} + \frac{\partial w}{\partial\theta}\right) \\ &+ RK_{66}\left(\frac{1}{R}\frac{\partial^2 u}{\partial x\partial\theta} + \frac{\partial^2 v}{\partial x^2}\right) - \frac{D_{12}}{R}\frac{\partial^3 w}{\partial x^2\partial\theta} \\ &+ \frac{D_{22}}{R^3}\left(\frac{\partial^2 v}{\partial\theta^2} - \frac{\partial^3 w}{\partial\theta^3}\right) + \frac{D_{66}}{2R}\left(\frac{\partial^2 v}{\partial x^2} - 2\frac{\partial^3 w}{\partial x^2\partial\theta}\right) \\ &- \frac{1}{R}N_{\theta 0}\left(v - \frac{\partial w}{\partial\theta}\right) + N_{x\theta 0}\frac{\partial w}{\partial x} = 0 \end{aligned} \tag{35b}$$

$$\begin{aligned} &RD_{11}\frac{\partial^4 w}{\partial x^4} - \frac{D_{12}}{R}\left(\frac{\partial^3 v}{\partial x^2\partial\theta} - 2\frac{\partial^4 w}{\partial x^2\partial\theta^2}\right) \\ &- \frac{D_{22}}{R}\left(\frac{\partial^3 v}{\partial\theta^3} - \frac{\partial^4 w}{\partial\theta^4}\right) - \frac{D_{66}}{R}\left(\frac{\partial^3 v}{\partial x^2\partial\theta} - 2\frac{\partial^4 w}{\partial x^2\partial\theta^2}\right) \\ &+ K_{12}\frac{\partial u}{\partial x} + \frac{K_{22}}{R}\left(\frac{\partial v}{\partial\theta} + w\right) - RN_{x0}\frac{\partial^2 w}{\partial x^2} \\ &+ \frac{N_{\theta 0}}{R}\left(\frac{\partial v}{\partial\theta} - \frac{\partial^2 w}{\partial\theta^2}\right) + N_{x\theta 0}\left(\frac{\partial v}{\partial\theta} - 2\frac{\partial^2 w}{\partial x\partial\theta}\right) = 0 \end{aligned} \tag{35c}$$

For the hygroscopic loading, the pre-buckling hygroscopic stresses are as in equations (12a) and (12b). Substituting equations (12) and (15) into equations (35a) to (35c), then setting the determinant of the coefficient equal to zero, moisture content can be deduced as below:

$$\begin{aligned} \Delta C = \Big\{ &\left(K_{11}\bar{m}^2 + K_{66}n^2\right) \\ &\times \left[\left(K_{66} + D_{66}/2R^2\right)\bar{m}^2 + \left(K_{22} + D_{22}/R^2\right)n^2\right] \\ &\times \left[D_{11}\bar{m}^4 + 2(D_{12} + D_{66})\bar{m}^2n^2 + D_{22}n^4 + K_{22}R^2\right] \\ &+ 2K_{12}(K_{12} + K_{66})n\bar{m}^2\left[(D_{12} + D_{66})n\bar{m}^2 \right.\\ &\left.+ D_{22}n^3 + K_{22}R^2n\right] - K_{12}^2\bar{m}^2 \\ &\times \left[\left(K_{66}R^2 + D_{66}/2\right)\bar{m}^2 + \left(K_{22}R^2 + D_{22}\right)n^2\right] \\ &- \left(K_{11}\bar{m}^2 + K_{66}n^2\right)\left[(D_{12} + D_{66})\bar{m}^2n \right.\\ &\left.+ D_{22}n^3 + K_{22}R^2n\right] \times \left[(D_{12} + D_{66})\bar{m}^2n/R^2 \right.\\ &\left.+ D_{22}n^3/R^2 + K_{22}n\right] - (K_{12} + K_{66})^2\bar{m}^2n^2 \\ &\times \left[D_{11}\bar{m}^4 + 2(D_{12} + D_{66})\bar{m}^2n^2 + D_{22}n^4 + K_{22}R^2\right]\Big\} \\ &\times \Big\{R^2\bar{m}^2(K_{11}\beta_1 + K_{12}\beta_2)\Big\{\left(K_{11}\bar{m}^2 + K_{66}n^2\right) \\ &\times \left[\left(K_{66} + D_{66}/2R^2\right)\bar{m}^2 + \left(K_{22} + D_{22}/R^2\right)n^2\right] \\ &- \bar{m}^2n^2(K_{12} + K_{66})^2\Big\}\Big\}^{-1} \end{aligned} \tag{36}$$

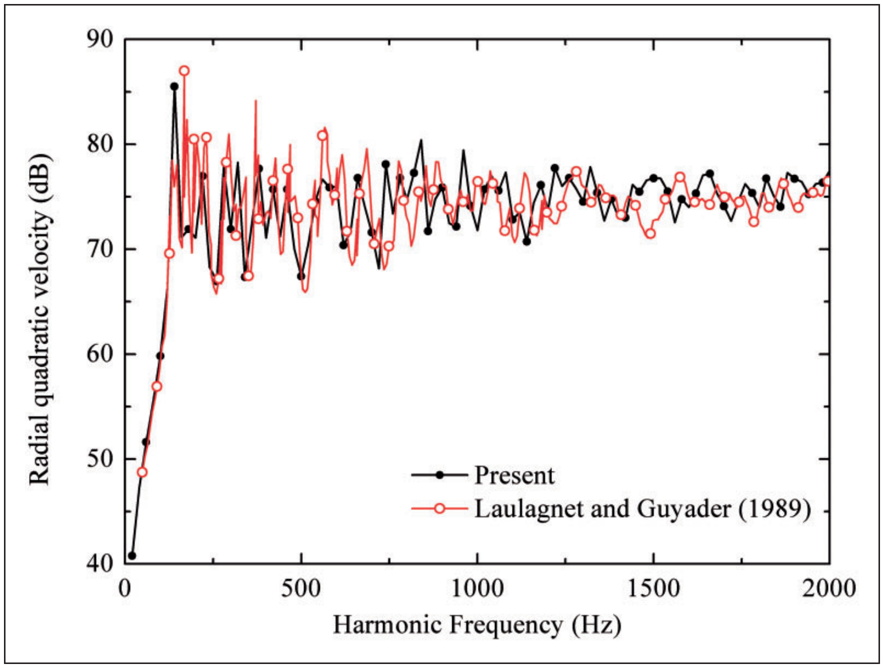

Figure 2. Comparison of radial quadratic velocity with Laulagnet and Guyader (1989).

As the variables m and n take a proper value respectively, the minimum value obtained from equation (36) is the critical buckling moisture content.

3. Validation studies

A simply supported finite isotropic cylindrical shell with dimensions $1.2\,m \times 0.4\,m \times 0.003\,m\,(L \times R \times h)$ analyzed by Laulagnet and Guyader (1989) is considered for the validation of radial quadratic velocity and radiated power calculation. The shell is made of steel with Young's modulus $E = 200\,GPa$, density $\rho = 7800\,kg/m^3$ and Poisson's ratio $\mu = 0.3$. The shell is assumed to be vibrating in air whose density is $1.21\,kg/m^3$ with a speed of sound $343\,m/s$. A harmonic excitation of 1 N is applied at $2L/5$ of the shell and a structure damping ratio of 0.01 is assumed of harmonic response analysis. The comparison of radial quadratic velocity and sound power level respectively with the results reported by Laulagnet and Guyader (1989) are shown in Figure 2 and Figure 3. It can be seen that the present results are in good agreement with those of Laulagnet and Guyader (1989) for radial quadratic velocity and sound power level, and then it could be said that the vibration and acoustic radiation model of the orthotropic cylindrical shell presented in the current paper is reliable and reasonable.

4. Results and discussion

In the present work, the vibration and acoustic response of an orthotropic cylindrical shell has been analyzed by assuming that the structure is subjected to a uniform moisture content rise above the ambient moisture content. The effects of different stiffness, length and thickness of the orthotropic cylindrical shell on the vibration and acoustic response are also studied.

An orthotropic composite cylindrical shell with the dimensions $0.6\,m \times 0.7\,m \times 0.0012\,m\,(L \times R \times h)$ which is excited at $(x_0 = L/2,\ \theta_0 = 0.0)$ by harmonic excitation with amplitude of 1 N in normal direction is now considered for a detailed investigation. The mechanical properties for the carbon-epoxy composites are assumed to be as follows:

$$E_1 = 172.5\,GPa, \quad E_2 = 34.5\,GPa,$$
$$G_{12} = E_2/2, \quad \mu_{12} = 0.25, \quad \rho = 1600\,kg/m^3,$$
$$\beta_1 = 0.0, \quad \beta_2 = 0.44$$

The density of the air (acoustic medium) is $\rho_0 = 1.21\,kg/m^3$ and the velocity of the sound is $c_0 = 343\,m/s$. The structure damping is equal to 0 without special explanation.

In order to obtain reasonable values of longitudinal and circumferential orders for convergence, the convergent check for the numerical solution in terms of the shell dimensions and material properties motioned above to sound power level is shown in Figure 4. It can be seen that sound power level is convergent until $m = 50$ and $n = 50$ in 0–1500 Hz frequency range, and in the higher frequency range, m and n should be chosen as a larger integer in order to obtain the convergent results.

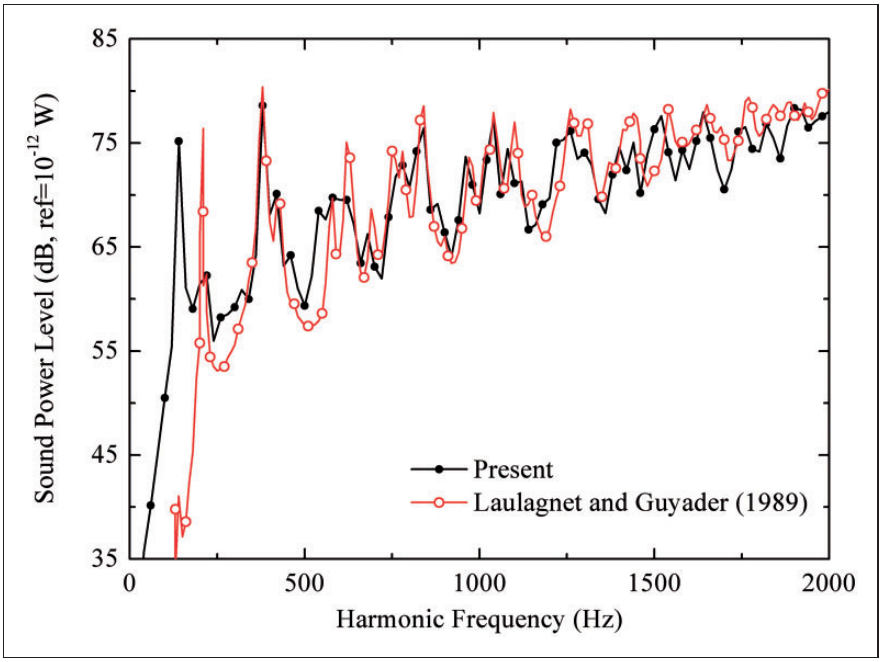

Figure 3. Comparison of sound power level with Laulagnet and Guyader (1989).

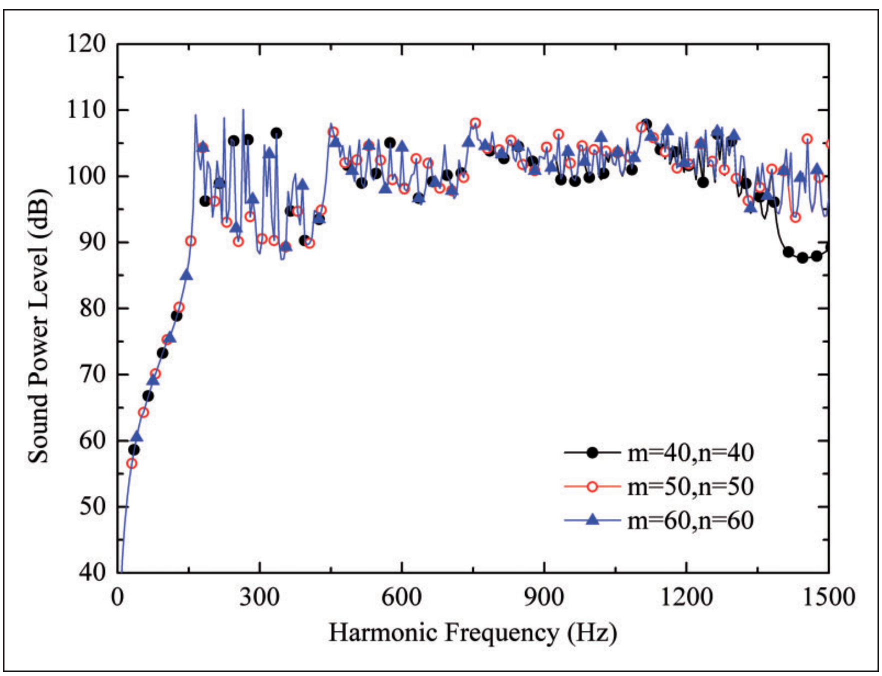

Figure 4. Convergence check of the numerical solution to sound power level.

4.1. Free vibration characteristics with incremental moisture contents

Initially, critical buckling moisture content is obtained and all the hygroscopic load cases are designed below the critical buckling moisture content. The moisture content rise applied on the shell is varied from 0.0% to C_{cr}(%) and corresponding variation in natural frequencies, mode shapes, vibration and acoustic response has been analyzed. According to Section 2.4 and substituting the parameters in equation (36), the critical buckling moisture content $C_{cr} = 1.30\%$ can be obtained as $m = 4$, $n = 22$.

Table 1. Natural frequencies (Hz) variation of first eight lowest frequency modes with moisture content.

Sl No.	$0C_{cr}$	$0.5C_{cr}$	$0.75C_{cr}$	$0.9C_{cr}$	$0.95C_{cr}$	$0.975C_{cr}$	$0.99C_{cr}$
1	165.3 (1,14)	128.2 (1,14)	105.1 (1,14)	88.5 (1,14)	81.7 (1,14)	78.6 (1,14)	62.5 (4,22)
2	166.6 (1,15)	129.9 (1,15)	107.1 (1,15)	90.8 (1,15)	84.2 (1,15)	81.2 (1,15)	71.6 (4,23)
3	168.9 (1,13)	132.8 (1,13)	110.6 (1,13)	94.9 (1,13)	88.7 (1,13)	85.8 (1,13)	76.5 (1,14)
4	172.2 (1,16)	136.9 (1,16)	115.5 (1,16)	100.5 (1,16)	94.6 (1,16)	91.9 (1,16)	78.4 (4,21)
5	177.8 (1,12)	143.9 (1,12)	123.7 (1,12)	109.9 (1,12)	104.6 (1,12)	95.7 (4,22)	79.2 (1,15)
6	181.5 (1,17)	148.3 (1,17)	128.8 (1,17)	115.5 (1,17)	110.4 (1,17)	100.3 (3,21)	83.9 (1,13)
7	192.5 (1,11)	161.6 (1,11)	143.9 (1,11)	132.2 (1,11)	116.4 (2,18)	101.9 (4,23)	84.3 (3,21)
8	193.9 (1,18)	163.1 (1,18)	145.5 (1,18)	133.9 (1,18)	117.2 (2,19)	102.2 (1,12)	90.2 (1,16)

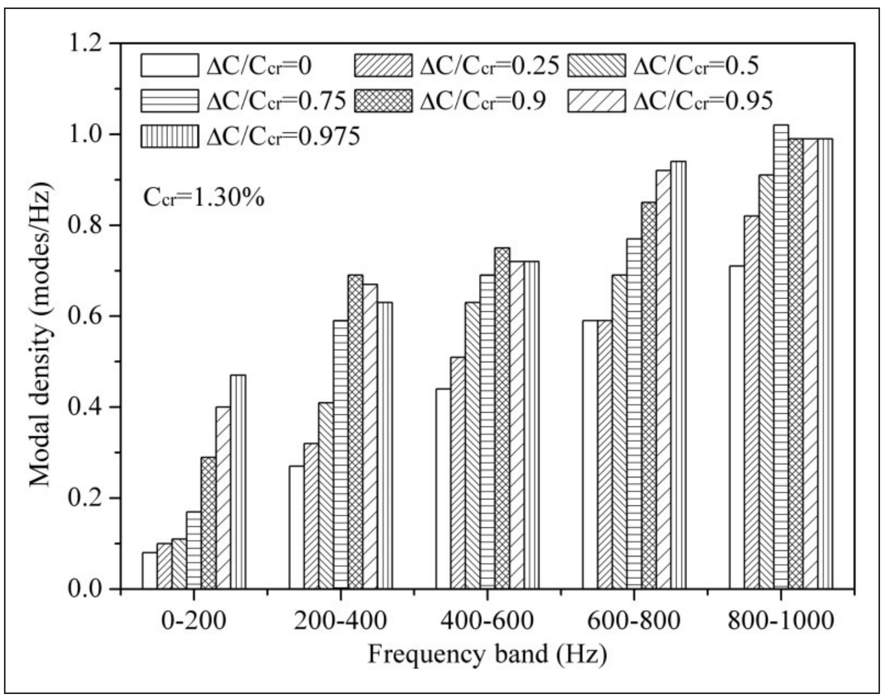

Figure 5. Modal density variation with moisture content in constant frequency band.

Firstly, the pre-stressed modal analysis is carried out for incremental uniform moisture contents ΔC in the orthotropic cylindrical shell from $0C_{cr}$, $0.5C_{cr}$, $0.75C_{cr}$, $0.9C_{cr}$, $0.95C_{cr}$, $0.975C_{cr}$ to $0.99C_{cr}$ to find the influence of hygroscopic environment on natural frequencies and corresponding mode shapes. The results obtained from the pre-stressed modal analysis are given in Table 1 which shows the lowest eight natural frequencies for various values of moisture content rise and the modal indices are stated in parentheses. It could be found that the natural frequencies generally reduce with an increase in uniform moisture content in the fraction of the critical moisture content and that the first natural frequency approaches zero as the uniform moisture content rise applied on the structure. In Table 1 it can be observed that the modal indices are changing with moisture content rise. The modal indices associated with the lowest frequency mode are (1, 14) at ambient moisture content and (4, 22) near the critical buckling moisture content. It can be seen from Table 1 that the axial and circumferential wave numbers associated with the lowest frequency mode reaches the modal indices corresponding to the lowest buckling mode due to uniform moisture content rise. This is because the stiffness of structure reduces with an increase in moisture content due to the compressive hygroscopic stresses.

As the natural frequencies associated with the thin cylindrical shell analyzed in the present work are close to each other, the natural frequencies in the excitation frequency range 0–1500 Hz are represented in terms of modal density (modes/Hz) in 200 Hz constant frequency bands. Modal density variation in 200 Hz

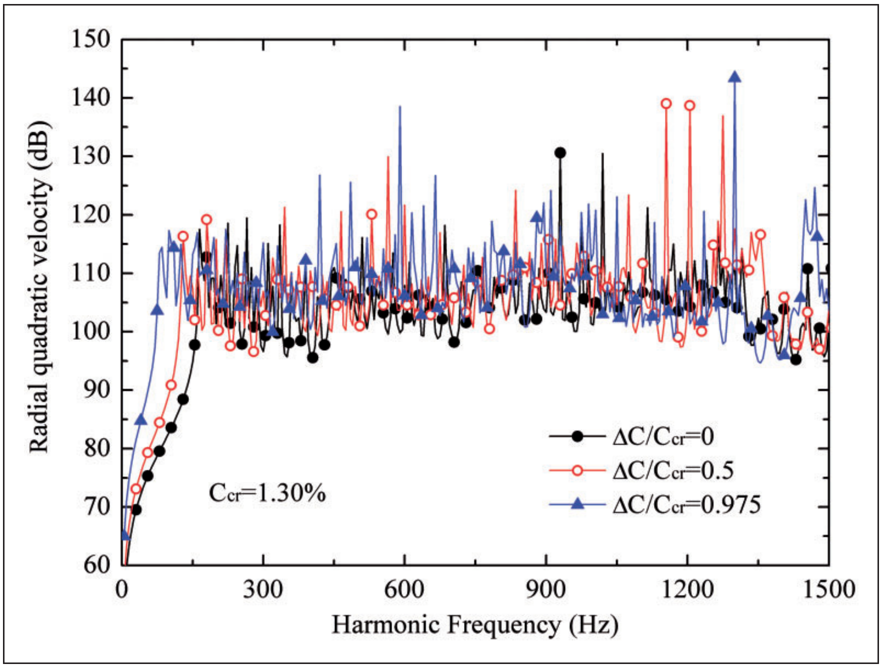

Figure 6. Radial quadratic velocity variation with moisture content.

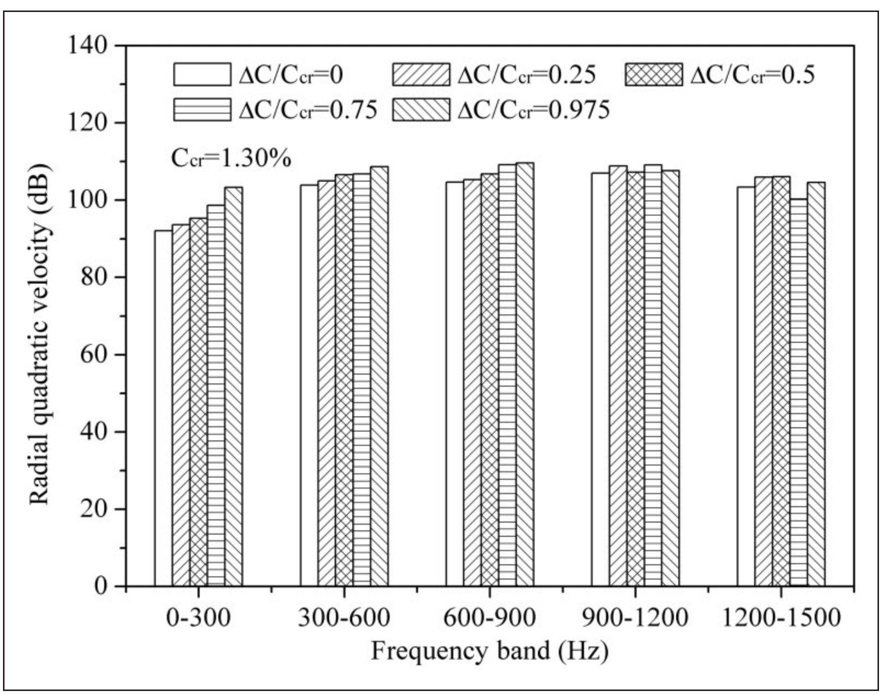

Figure 7. Radial quadratic velocity in constant frequency band.

frequency band is shown in Figure 5. Shifting of natural frequencies towards lower frequency band can be clearly seen in the 0–200 Hz band; this is the reason that the natural frequencies decrease with the moisture content which results in the number of modal increases in the lower frequency band.

4.2. Vibration and sound radiation characteristics with incremental moisture contents

In order to compare the vibration response and sound characteristics, a frequency range of 0–1500 Hz is chosen for different moisture content.

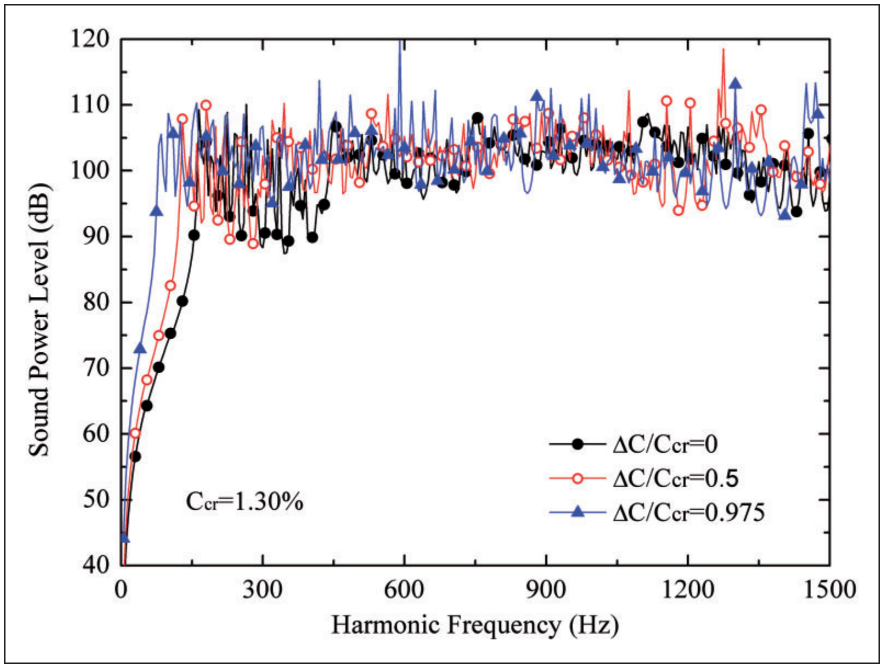

Figure 8. Sound power level variation with moisture content.

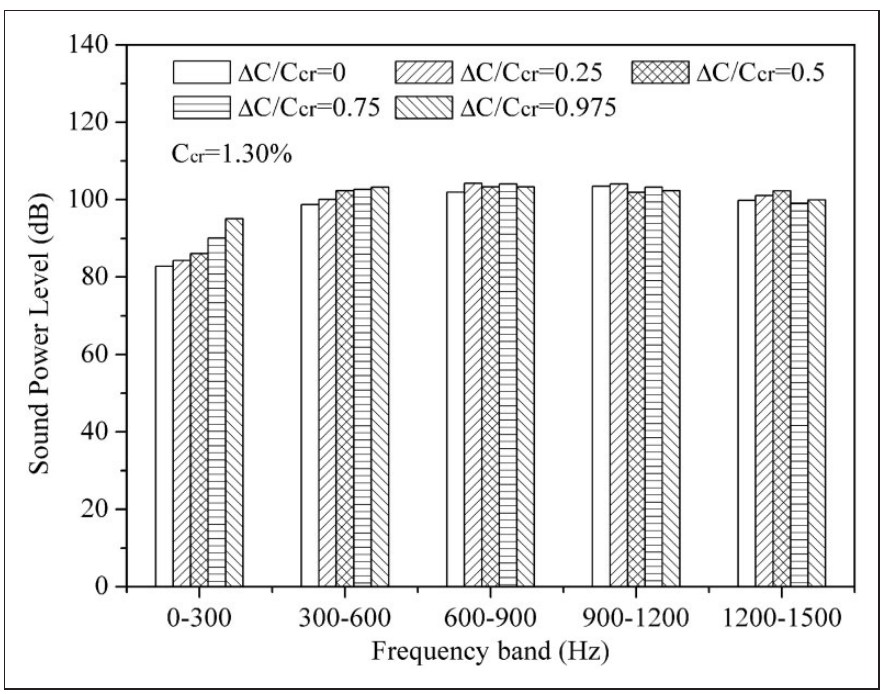

Figure 9. Sound power level variation with moisture content in constant frequency band.

Figure 6 shows the radial quadratic velocity of the orthotropic shell with $0C_{cr}$, $0.5C_{cr}$ and $0.975C_{cr}$ moisture contents. The plot describes the radial quadratic velocity, which appears to shift to low frequencies with the moisture content, and that the shifting of the first peak associated with the fundamental frequency towards lower frequency direction can be clearly observed. It is the reason that the natural frequency decreases with the increase of moisture content, then the resonance peaks in each natural frequency will float to low frequency direction.

The radial quadratic velocity in constant frequency bands (300 Hz) (300 Hz has been chosen to have five constant frequency bands in 0–1500 Hz) for

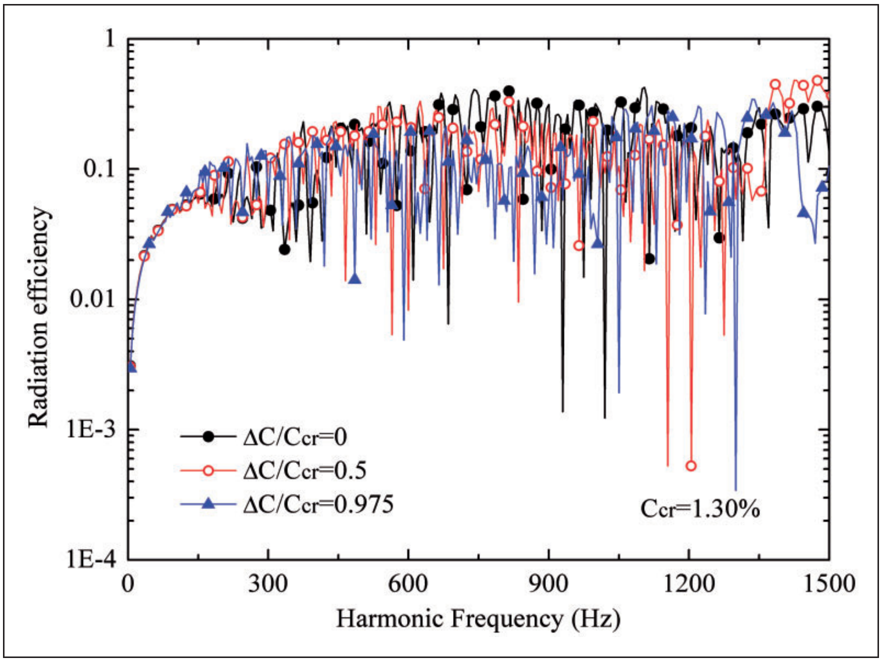

Figure 10. Radiation efficiency variation with moisture content.

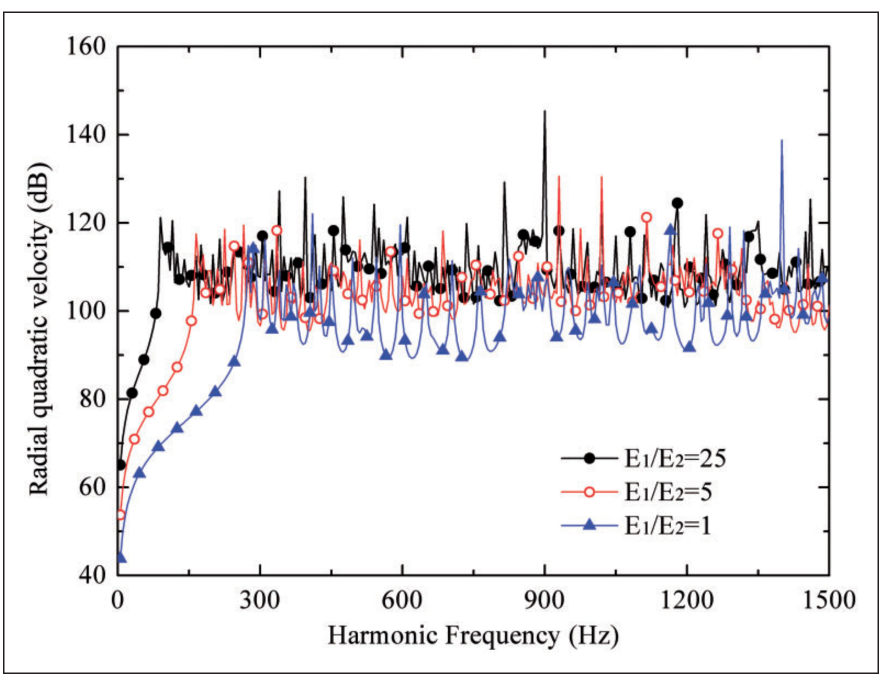

Figure 11. Radial quadratic velocity variation with the stiffness.

various moisture content rises has been obtained and shown in Figure 7. An increase in radial quadratic velocity in the lower frequency bands can be observed.

Figure 8 and Figure 9 show the sound power level of the orthotropic shell with $0C_{cr}$, $0.5C_{cr}$ and $0.975C_{cr}$ moisture content. As well as the trend in Figure 6 and Figure 7, the first peak of sound power level floats to

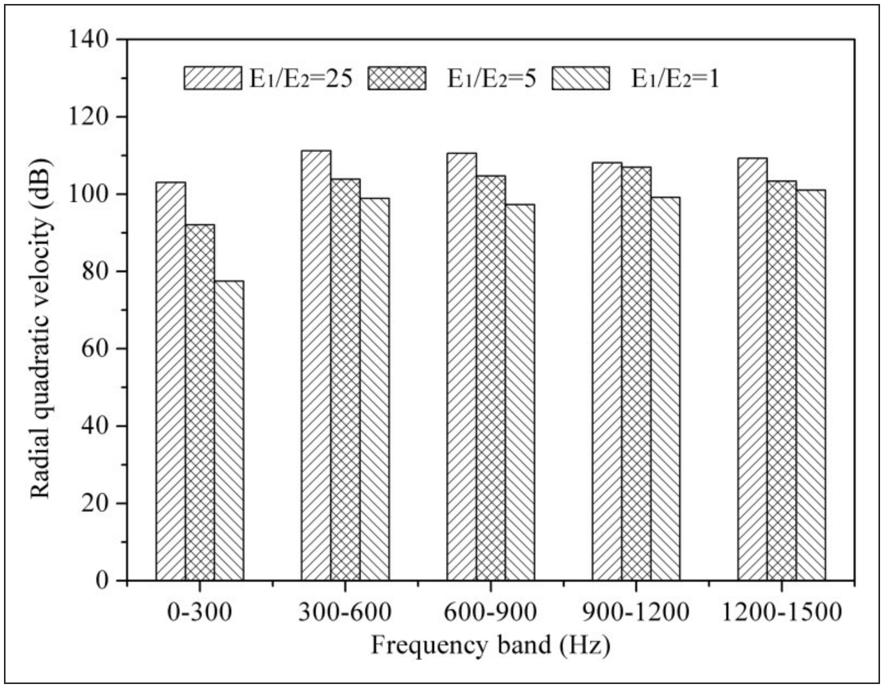

Figure 12. Radial quadratic velocity variation with the stiffness in constant frequency band.

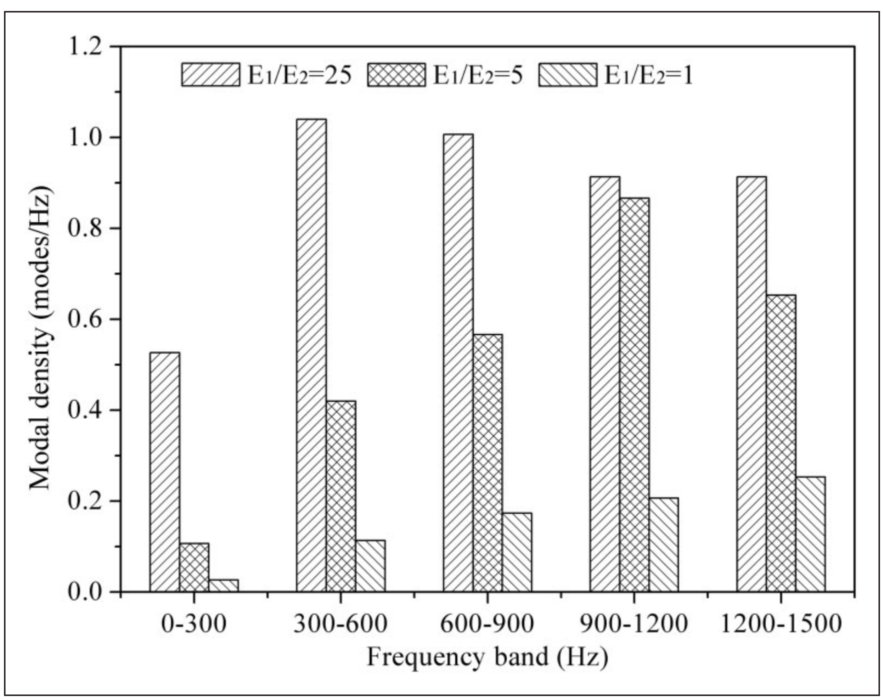

Figure 13. Modal density variation with stiffness in constant frequency band.

the lower frequency direction and increases in the lower frequency bands due to the decrease of natural frequency with moisture content. It indicates that the sound power radiated depends on the radial velocity of the vibrating cylindrical shell.

The sound radiation efficiency of the orthotropic shell as a function of frequency is plotted in Figure 10. It is quite clear that radiation efficiency generally decreases with moisture content (no significant variation in lower frequencies).

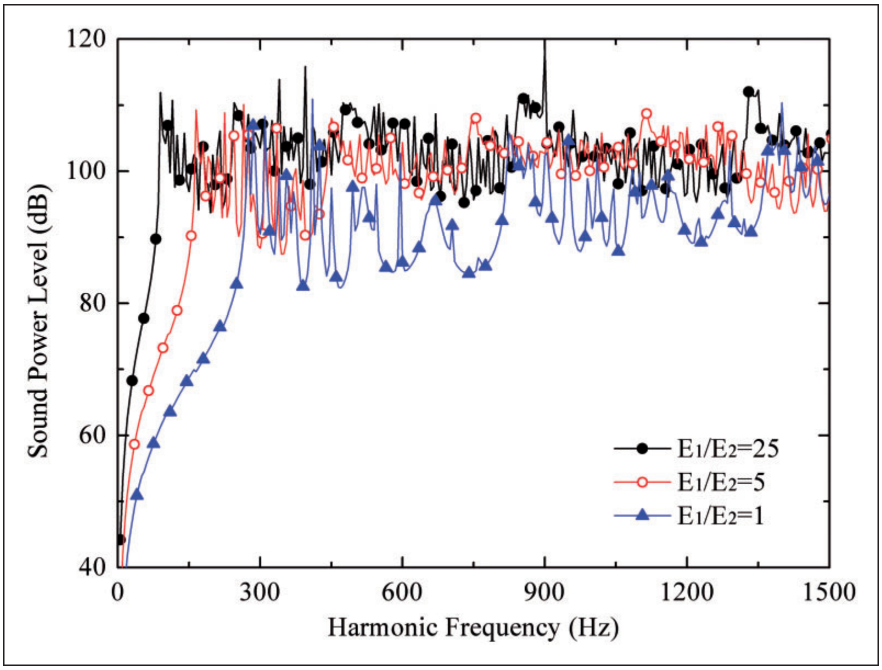

Figure 14. Sound power level variation with the stiffness.

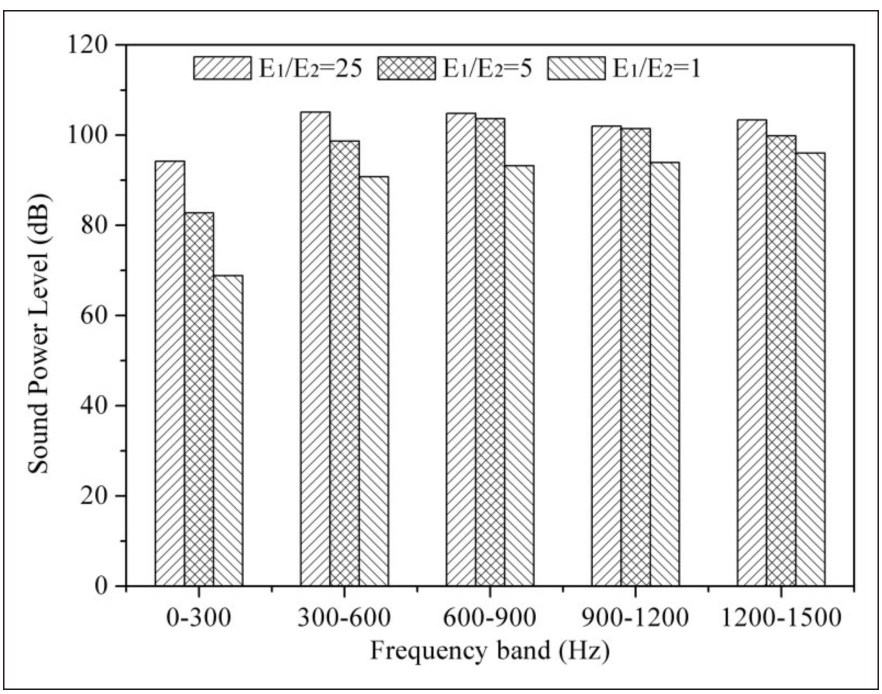

Figure 15. Sound power level variation with the stiffness in constant frequency band.

4.3. Vibration and sound radiation characteristics with different stiffness

In this section, to research the effects of different stiffness on the vibration and acoustic responses of the orthotropic shell, the Young's modulus E_1 is kept unchanged in 172.5 GPa while assigning Young's modulus E_2 artificially increases from 6.9, 34.5 to 172.5 GPa, and then the general stiffness of the orthotropic shell increases gradually as the ratio of E_1 to E_2 reduces from 25, 5 to 1. When the ratio reduces to one, the orthotropic shell is equivalent to an isotropic shell approximately.

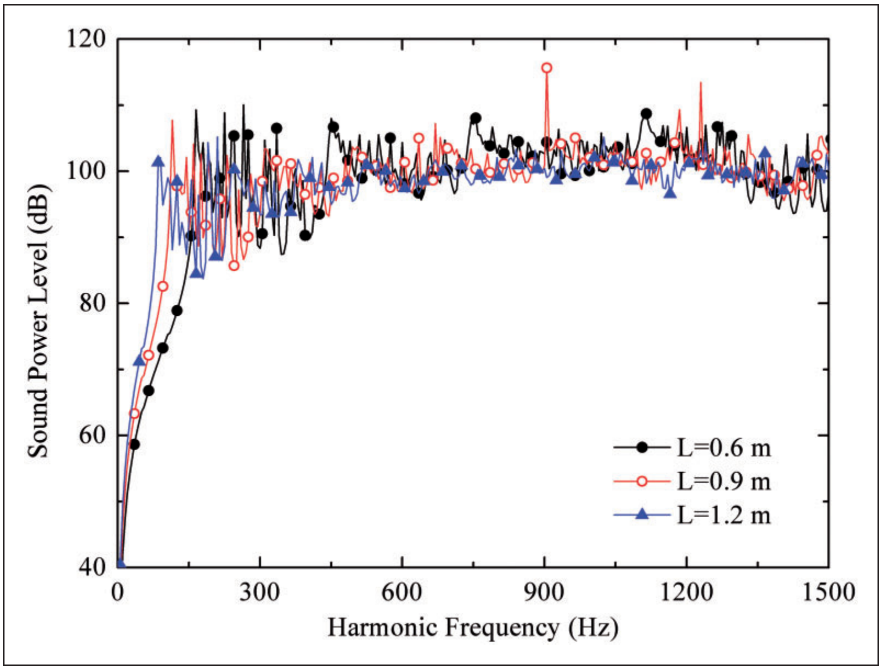

Figure 16. Sound power level variation with the length.

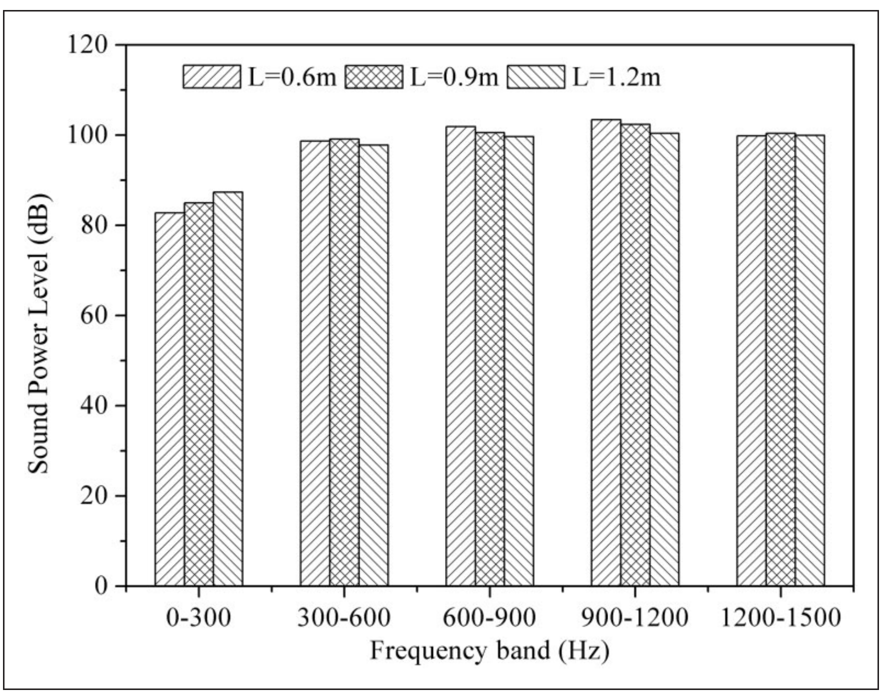

Figure 17. Sound power level variation with the length in constant frequency band.

The effects of the different stiffness on the radial quadratic velocity of ation and acoustic responses The effects of the different stiffness on the radial quadratic velocity of the orthotropic shell are shown in Figure 11 and Figure 12. It can be seen from Figure 11 that the shifting of the first peak associated with the fundamental frequency towards higher frequency direction, which indicates that the fundamental frequency increases with the increase of the stiffness, and the amplitude of the velocity increasing with the stiffness are also observed clearly. The plot in Figure 12 indicates that the radial quadratic velocity decreases with the

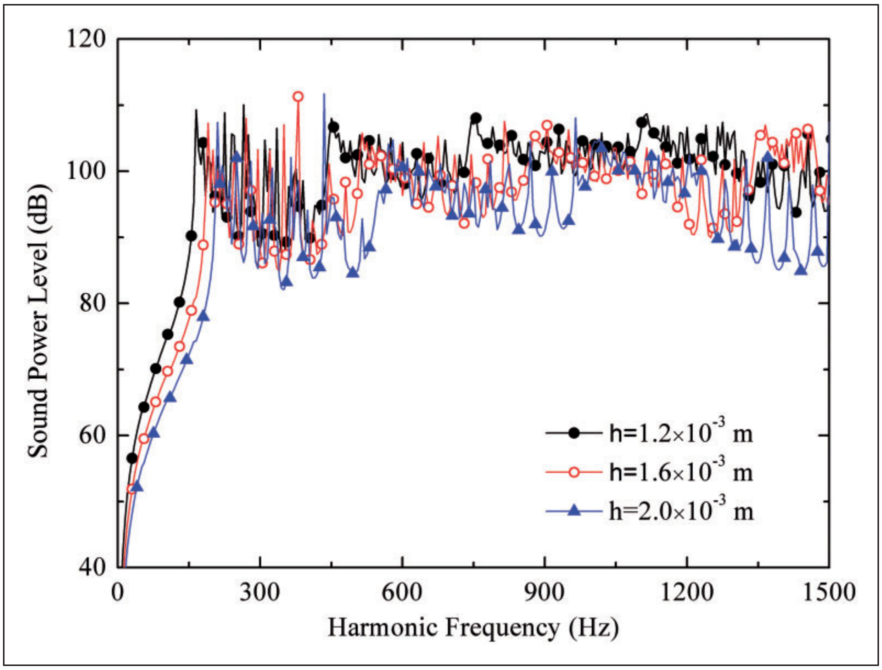

Figure 18. Sound power level variation with the thickness.

decreasing ratio in the whole frequency band (significant variation in lower frequencies). It can be observed in Figure 11 that the peaks in resonance modes reduce in the 1–1500 Hz range with the enhancement of the stiffness due to the decreasing ratio of E_1/E_2, and the modal density variation with stiffness in constant frequency band can be clearly seen in Figure 13. The modal density reduces with the incremental stiffness which results in that the radial quadratic velocity decreases with the decreasing ratio of elasticity modulus.

Sound power level and sound power level in constant frequency band of the different ratio of the elastic modulus illustrated in Figure 14 and Figure 15 show trends similar to radial quadratic velocity.

4.4. Sound radiation characteristics with different length and thickness

The sound power level of the orthotropic cylindrical shell with different length and thickness is presented to research the effects of different length and thickness on the acoustic response. The initial dimensions of the cylindrical shell are $0.6\,m \times 0.7\,m \times 0.0012\,m$ ($L \times R \times h$). Firstly, the length increases from $0.6\,m$, $0.9\,m$ to $1.2\,m$ and the radial and thickness are kept unchanged to research the influence of the variation of the length on the acoustic response. Secondly, the thickness increases from $0.0012\,m$, $0.0016\,m$ to $0.002\,m$ but the radial and length are kept unchanged to research the influence of the thickness variation on the acoustic radiation.

The sound power level and that in constant frequency band of different length for the orthotropic cylindrical shell are shown in Figure 16 and Figure 17. The shifting of the first peak to the lower frequency can be observed in Figure 16, which indicates that the fundamental frequency of the orthotropic cylindrical shell decreases with the length. It can also be observed in Figure 17 that the change of length has little impact on the sound radiation for the orthotropic cylindrical shell, especially in the higher frequency band.

The sound power level and that in constant frequency band of orthotropic cylindrical shell for different thickness are shown in Figure 18 and Figure 19. The shifting of the first peak to the higher frequency can be observed in Figure 18, which indicates that the fundamental frequency of the orthotropic cylindrical shell increases with the thickness as a result of the increasing stiffness. It can also be observed in Figure 19 that the sound radiation decreases with the thickness in the whole frequency band.

5. Conclusions

The current paper carried out an analytical study considering the hygroscopic effect on the vibration response and acoustic radiation of a finite thin orthotropic composite shell excited by a harmonic concentrated force. A theoretical solution considering the effects of hygroscopic stress and mass addition caused by moisture absorption is obtained. First, to verify the theoretical model, radial quadratic velocity and sound

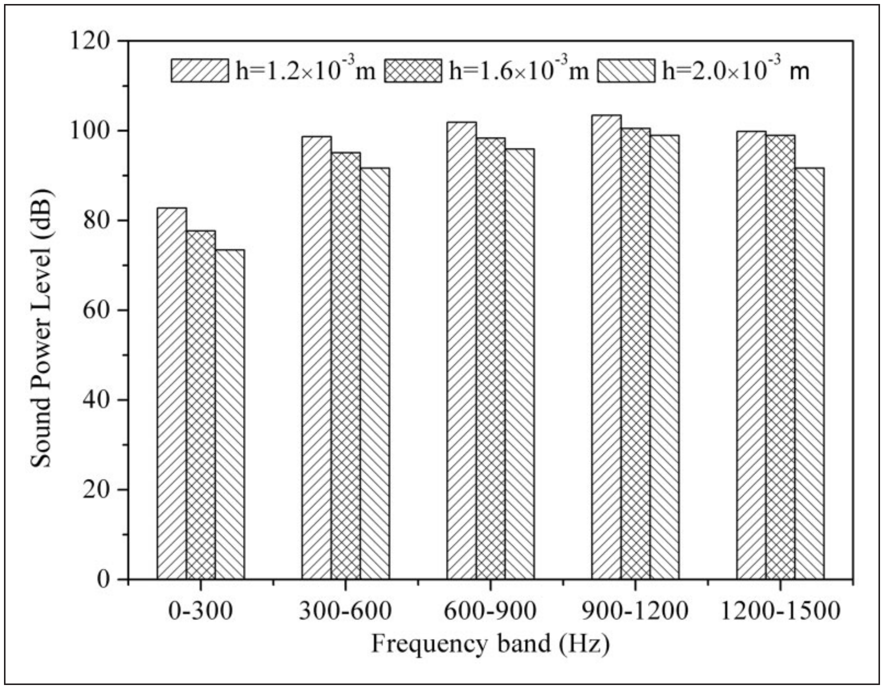

Figure 19. Sound power level variation with the thickness in constant frequency band.

power level are validated by the results available in the literature for the isotropic cylindrical shell. Second, with the critical buckling moisture content as a parameter, the natural frequencies, radial quadratic velocity, sound power and radiation efficiency with incremental moisture content are computed respectively. Third, the decreasing ratios of longitudinal Young's modulus to the tangential are set artificially to study the vibration and acoustic radiation characteristics with the different stiffness of the orthotropic shell. Finally, the sound power level is studied with the different length and thickness of the orthotropic cylindrical shell.

From the natural vibration analysis, it could be found that the natural frequencies decrease with the increase of the moisture content. The modal indices associated with the lowest frequency mode reaches the modal indices corresponding to the lowest buckling mode near the critical buckling moisture content due to uniform moisture content rise. The radial quadratic velocity and sound power increase, but radiation efficiency generally decreases with the incremental moisture content. In the analysis for the effect of different stiffness on vibration and acoustic responses of the orthotropic cylindrical shell, the radial quadratic velocities, sound power and radiation efficiency decrease with the decreasing ratio of longitudinal Young's modulus to the tangential modulus, while the fluctuation of the responses' amplitude increases with the decreasing ratio. The variation of the length has little impact on the sound radiation of the orthotropic cylindrical shell. The acoustic response attenuates with the increasing thickness.

Funding

This work is supported by the National Natural Science Foundation of China (grant numbers 11321062, 11472206 and 91016008).

References

Brush DO and Almroth BO (1975) *Buckling of Bars, Plates and Shells*. New York: McGraw-Hill.

Burroughs CB (1984) Acoustic radiation from fluid-loaded infinite circular cylinders with doublyperiodic ring supports. *Journal of the Acoustical Society of America* 75(4): 715–722.

Cao X, Hua H and Ma C (2012) Acoustic radiation from shear deformable stiffened laminated cylindrical shells. *Journal of Sound and Vibration* 331: 651–670.

Civalek O (2013) Vibration analysis of laminated composite conical shells by the method of discrete singular convolution based on the shear deformation theory. *Composite Part-B: Engineering* 45: 1001–1009.

Civalek O and Gürses M (2009) Free vibration analysis of rotating cylindrical shells using discrete singular convolution technique. *International Journal of Pressure Vessels and Piping* 86(10): 677–683.

Daneshjou K, Nouri A and Talebitooti R (2009) Analytical model of sound transmission through orthotropic cylindrical shells with subsonic external flow. *Aerospace Science and Technology* 13: 18–26.

Eslami MR, Ziaii AR and Ghorbanpour A (1996) Thermal elastic buckling of thin cylindrical shells based on improved stability equations. *Journal of Thermal Stresses* 19: 299–315.

Eslami MR and Javaheri R (1999) Buckling of composite cylindrical shells under mechanical and thermal loads. *Journal of Thermal Stresses* 22: 527–545.

Jeyaraj P, Padmanabhan C and Ganesan N (2008) Vibration and acoustic response of an isotropic plate in a thermal environment. *Journal of Vibration and Acoustics* 130: 051005–051006.

Jeyaraj P, Padmanabhan C and Ganesan N (2011) Vibro-acoustic response of a circular isotropic cylindrical shell under a thermal environment. *International Journal of Applied Mechanics* 3(3): 525–541.

Junger MC and Feit D (1986) *Sound, Structures, and Their Interaction*, 2nd ed. London, UK: MIT Press.

Kaw AK (2006) *Mechanics of Composite Materials*, 2nd ed. Boca Raton, FL: Taylor & Francis.

Laulagnet B and Guyader JL (1989) Modal analysis of a shell's acoustic radiation in light and heavy fluids. *Journal of Sound and Vibration* 131(3): 397–415.

Leissa AW (1973) *Vibration of Shells*. Washington, DC: NASA SP-288.

Liao C-J, et al. (2011) Vibration and sound radiation from submerged finite cylindrical shells reinforced with axially periodic stiffeners. *Journal of Vibration and Control* 17(10): 1472–1480.

Lyrintzis CS and Bofilios DA (1990) Hygrothermal effects on structure-borne noise transmission of stiffened laminated composite plates. *Journal of Aircraft* 27(8): 722–730.

Naidu SNV and Sinha PK (2007) Nonlinear free vibration analysis of laminated composite shells in hygrothermal environments. *Composite Structures* 77: 475–483.

Parhi PK, Bhattacharyya SK and Sinha PK (2001) Hygrothermal effects on the dynamic behavior of multiple delaminated composite plates and shells. *Journal of Sound and Vibration* 248(2): 195–214.

Rdzanek WP, Rdzanek WJ and Szemela K (2014) The low frequency axisymmetric modal sound radiation efficiency of an elastically supported annular plate. *Journal of Sound and Vibration* 333(1): 144–165.

Shen H (2001) The effects of hygrothermal conditions on the postbuckling of shear deformable laminated cylindrical shells. *International Journal of Solid and Structures* 38: 6357–6380.

Soedel W (2004) *Vibrations of Shells and Plates*, 3rd ed. New York: Marcel Dekker, Inc.

Stepanishen PR (1982) Modal coupling in the vibration of fluid-loaded cylindrical shells. *Journal of the Acoustical Society of America* 71(4): 813–823.

Wang C and Lai JCS (2000) The sound radiation efficiency of finite length acoustically thick circular cylindrical shells under mechanical excitation I: theoretical analysis. *Journal of Sound and Vibration* 232(2): 431–447.

Wang C and Lai JCS (2001) The sound radiation efficiency of finite length acoustically thick circular cylindrical shells under mechanical excitation II: Limitations of the infinite length model. *Journal of Sound and Vibration* 241(5): 825–838.

Whitney JM and Ashton JE (1971) Effect of environment on the elastic response of layered composite plates. *American Institute of Aeronautics and Astronautics Journal* 9(9): 1708–1713.

Xie G and Luo D (1995) Analytical solution of radiated sound pressure of ring-stiffened cylindrical shells in fluid medium. *Ship Building of China* 131(4): 37–45.

Zhang LW and Liew KM (2014a) An element-free based solution for nonlinear Schrödinger equations using the ICVMLS–Ritz method. *Applied Mathematics and Computation* 249: 333–345.

Zhang LW and Liew KM (2014b) An improved moving least-squares Ritz method for two-dimensional elasticity problems. *Applied Mathematics and Computation* 246: 268–282.

Zhang LW, et al. (2014) The improved complex variable element-free Galerkin method for two-dimensional Schrödinger equation. *Computers & Mathematics with Applications* 68: 1093–1106.

Zhao X, Geng Q and Li Y (2013) Vibration and acoustic response of an orthotropic composite laminated plate in a hygroscopic environment. *Journal of the Acoustical Society of America* 133(3): 1433–1442.